

## Multiple time scale blinking in InAs quantum dot single-photon sources

Marcelo Davanço,<sup>1,2,\*</sup> C. Stephen Hellberg,<sup>3,†</sup> Serkan Ates,<sup>1,2</sup> Antonio Badolato,<sup>4</sup> and Kartik Srinivasan<sup>1,‡</sup>

<sup>1</sup>*Center for Nanoscale Science and Technology, National Institute of Standards and Technology, Gaithersburg, Maryland 20899, USA*

<sup>2</sup>*Maryland NanoCenter, University of Maryland, College Park, Maryland 20742, USA*

<sup>3</sup>*Center for Computational Materials Science, Code 6390, Naval Research Laboratory, Washington, DC 20375, USA*

<sup>4</sup>*Department of Physics and Astronomy, University of Rochester, Rochester, New York 14627, USA*

(Received 3 June 2013; revised manuscript received 3 April 2014; published 16 April 2014; publisher error corrected 17 April 2014)

We use photon correlation measurements to study blinking in single, epitaxially grown self-assembled InAs quantum dots situated in circular Bragg grating and microdisk cavities. The normalized second-order correlation function  $g^{(2)}(\tau)$  is studied across 11 orders of magnitude in time, and shows signatures of blinking over time scales ranging from tens of nanoseconds to tens of milliseconds. The  $g^{(2)}(\tau)$  data is fit to a multilevel system rate equation model that includes multiple nonradiating (dark) states, from which radiative quantum yields significantly less than 1 are obtained. This behavior is observed even in situations for which a direct histogramming analysis of the emission time-trace data produces inconclusive results.

DOI: [10.1103/PhysRevB.89.161303](https://doi.org/10.1103/PhysRevB.89.161303)

PACS number(s): 78.67.Hc, 78.55.Cr, 81.07.Ta, 85.35.Be

Single-photon sources based on single epitaxially grown quantum dots (QDs) are promising devices for photonic quantum information science [1,2]. As single-photon source brightness is crucial in many applications, III-V compound nanostructures like InAs QDs in GaAs are of particular interest, both due to their short radiative lifetimes (typically  $\approx 1$  ns [3]) and the availability of mature device fabrication technology for creating scalable nanophotonic structures which can modify the QD radiative properties in desirable ways. In particular, structures can be created to further increase the QD radiative rate [4] and funnel a large fraction of the emitted photons into a desired collection channel [5].

The overall brightness of the source is, however, also influenced by the radiative efficiency of the QD, which can deviate from unity for a variety of reasons, including coupling of the radiative transition to nonfluorescing states. Such fluorescence intermittency, also called blinking, is an apparently ubiquitous phenomenon in solid-state quantum emitters [6–9], being particularly pronounced in single nanocrystal QDs and organic molecules. In contrast, blinking in epitaxially grown III-V QDs has not received as much attention, largely due to the fact that such QDs, grown in ultrahigh-vacuum environments and embedded tens of nanometers below exposed surfaces, typically do not express pronounced fluorescence intermittency [10,11]. Obvious blinking (at the  $\approx 100$  ms to  $\approx 1$  s time scales) has only been observed in InGaAs QDs grown close to crystal defects [12] and in some InP QDs [13,14]. Submicrosecond blinking dynamics in InAs QDs have also been studied [15].

Here, we study blinking in InAs/GaAs QDs embedded in photonic nanostructures that enable high collection efficiencies ( $\approx 10\%$ ) [16,17]. As these devices do not exhibit pronounced fluorescence variations, we use photon correlation measurements [18] as a more informative approach to investigate blinking over time scales ranging from tens of nanoseconds to hundreds of milliseconds. The data is fit with a multilevel

rate equation model for the QD that yields estimates for the transition rates and occupancies of the QD states, enabling an overall estimate of the QD radiative efficiency. Notably, we find quantum yields significantly less than 1 even in QDs which show no blinking in histogramming analysis. This information is valuable in quantifying the extraction efficiency of QD emission, and in understanding the ultimate brightness achievable for QD single-photon sources. We anticipate that the importance of this topic is likely to grow as epitaxially grown QDs are incorporated within photonic nanostructures with critical dimensions of tens of nanometers, at which point surfaces play an important role [19].

Our samples consist of InAs QDs embedded in the center of a 190-nm-thick GaAs layer. The collection efficiency of emitted photons is enhanced through the use of a circular grating microcavity [16,17] or fiber-coupled microdisk cavity geometry [20], as detailed in the Supplemental Material [21]. The devices are cooled to 10 K in a liquid helium flow cryostat and excited by a 780-nm (above the GaAs band gap) continuous wave laser. The collected emission is spectrally filtered (bandwidth  $< 0.2$  nm  $\approx 250$   $\mu$ eV) to select a single state of a single QD (typically the biexciton or neutral exciton state), split on a 50/50 beam splitter, and sent to a pair of silicon single-photon counting avalanche diodes (SPADs) [see Fig. 1(a)]. The SPAD outputs are directed to a time correlator that records photon arrival times for each channel with a resolution of 4 ps. Data is typically recorded over a period of 1 h. Results from three different devices (labeled 1,2,3) are described below.

Figure 2(a) shows a portion of the fluorescence time trace recorded from device 1, where detection events are binned into 3 ms bins. The time-trace data clearly show a fluctuating fluorescence intensity, more often exhibiting high rather than low levels. This is further seen in the histogram of detection events per bin shown next to the time trace, which exhibits a bimodal behavior biased towards the higher count rates. Figures 2(b) and 2(c) show the corresponding time-trace and histogram data for 20 and 100 ms time bins. At the 20 ms bin width, a bimodal distribution in the histogram is more clearly seen. At 100 ms, it becomes less visible, as is the contrast between high and low intensities in the time trace. When the

\*marcelo.davanco@nist.gov

†steve.hellberg@nrl.navy.mil

‡kartik.srinivasan@nist.gov

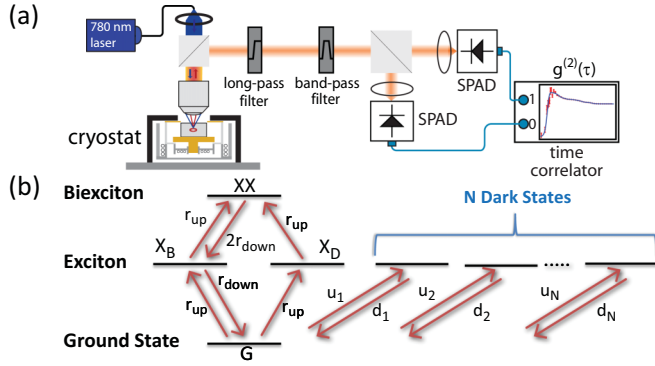


FIG. 1. (Color online) (a) Experimental setup. (b) Multilevel model with  $N$  dark states used to describe the QD behavior. Pumping into the “bright” and “dark” single excitonic states ( $X_B$  and  $X_D$ ) from the ground state ( $G$ ), and the biexciton state ( $XX$ ) from the single exciton states, occurs at a rate  $r_{up}$ . Spontaneous emission from the biexciton (exciton) state occurs at a rate  $2r_{down}$  ( $r_{down}$ ). The up-transition (down-transition) rates between the ground state and dark states are labeled  $u_i$  ( $d_i$ ), where  $i=1 \dots N$ .

bin width is increased to 1000 ms, obvious signs of blinking are no longer observable in either the time-trace or histogram data [21].

The sensitivity of time-trace and histogram data to the choice of bin width is well known [18,22,23], and can limit the ability to achieve a complete picture of the system dynamics. In particular, the minimum reliable bin size is limited by the available photon flux and the shot noise, while too large bin sizes average out fluctuations occurring at shorter time scales. Histogram analysis of the high or low fluorescence level time interval distributions is furthermore influenced by the selection of a threshold intensity level. In contrast, intensity autocorrelation analysis does not require such potentially arbitrary input parameters. In Fig. 2(d), we plot the intensity autocorrelation function  $g^{(2)}(\tau)$  for device 1 over a time range exceeding 11 orders of magnitude (error bars are due to fluctuations in the detected photon count rates, and represent one standard deviation [21]). This data, calculated using an efficient approach [21] similar to that described in Ref. [24], indicates that the photon antibunching at  $\tau = 0$ , expected for a single-photon emitter, is followed by photon bunching that peaks in the 10 ns region before slowly decaying, with  $g^{(2)}(\tau) = 1$  only occurring for  $\tau > 0.1$  s [see zoomed-in data in Fig. 2(e)]. The decay in  $g^{(2)}(\tau)$  is punctuated by a series of inflection points (“shoulders”) in which the concavity of the curve changes. Such features have been observed in fluorescence autocorrelation curves of single aromatic molecules in polymeric hosts [25,26]. Photon bunching in these systems arises from shelving of the molecule into dark triplet states, resulting in bursts of emitted photons followed by dark intervals at characteristic rates. Similar behavior can also originate from interactions between the molecule and neighboring two-level systems (TLS) in the host polymer. Switching between the states of the TLS leads to sudden jumps in emission frequency, and correspondingly, emission intensity. Multiple shoulders in the autocorrelation have been associated with coupling to a number of TLSs with varying switching rates.

We interpret our  $g^{(2)}(\tau)$  data similarly, taking the radiative QD transition to be coupled to multiple nonradiative, or dark, states [21], as depicted in Fig. 1(b). This phenomenological model is motivated by potential physical mechanisms present in self-assembled InAs/GaAs QDs. For example, lattice defects in the vicinity of the QD can act as carrier traps, and charge tunneling events between the QD and such traps lead to fluorescence intermittency [12,13]. Perturbation of the electron and hole wave function overlap by the local electric field of trapped charges has also been postulated as a cause of blinking [14]. Another possibility is that tunneling of carriers into nearby traps causes spectral shifts of the QD emission out of the  $\approx 0.2$  nm filter bandwidth, leading to an effective blinking behavior. Such shifts would, however, be larger than the spectral diffusion measurements recently reported [27–30]. We did not observe such spectral diffusion in spectroscopy with a 0.035 nm resolution.

In these scenarios, interactions with surrounding traps drive the QD into high or low emission states with well-defined rates, consistent with the model of Fig. 1(b). Here, each dark state  $i$  is populated at a rate  $u_i$  and depopulated at a rate  $d_i$ . We solve the rate equations to compute  $g^{(2)}(\tau)$  using the appropriate transition for each device: the  $XX \rightarrow X_B$  transition for devices 1 and 2, and the  $X_B \rightarrow G$  transition for device 3. All parameters are varied in the fit except for the radiative decay rate,  $r_{down}$ , which is determined from independent measurements [21]. A first estimate of the number of dark states used in the model is the number of shoulders in the measured  $g^{(2)}(\tau)$  data. Ultimately, the number of dark states is determined by the  $\chi^2$  parameter minimized in the fit, as defined in [21].

Fits to device 1 data are shown as blue solid lines in Figs. 2(d) and 2(e), along with extracted occupancy and population and depopulation rates,  $u_i$  and  $d_i$ , of each dark state. The short ( $< 10$  ns) time behavior of  $g^{(2)}(\tau)$  depends primarily on the excitation rate  $r_{up}$ , the decay rate  $r_{down}$ , the SPAD timing jitter, and the background signal, if present [21]. The behavior at longer times depends primarily on  $u_i$  and  $d_i$ . Accurate fits require a minimum number  $N$  of dark states (eight for this device), below which the behavior of  $g^{(2)}(\tau)$ , quantified by the fit  $\chi^2$ , is not well reproduced. Larger  $N$  has negligible impact on the fit [Fig. 2(f)], and the total dark state occupancy changes by  $< 0.05\%$ . The radiative quantum yield (radiative efficiency) is estimated by subtracting this total dark state occupancy from unity. We note that as the rate coupling states  $G$ ,  $X_B$ ,  $X_D$ , and  $XX$  are more than an order of magnitude faster than rates to the dark states, the quality of the fits and the resulting quantum yield does not depend on whether the dark states are coupled to  $G$  (Fig. 1) or  $X_B$ . Similarly, replacing the dark states with partially emissive gray states [31], modeled with a branching ratio between dark and bright transitions, does not significantly affect the fits or computed quantum yield [21].

In all, the  $g^{(2)}(\tau)$  data and rate equation analysis uncover qualitatively new information about blinking in this device in comparison to the time-trace and histogram data. First, we see that blinking occurs across a wide variety of time scales. While blinking at submicrosecond time scales has been reported in epitaxially grown InAs QDs previously [15,32], our measurements show that these systems can exhibit blinking out

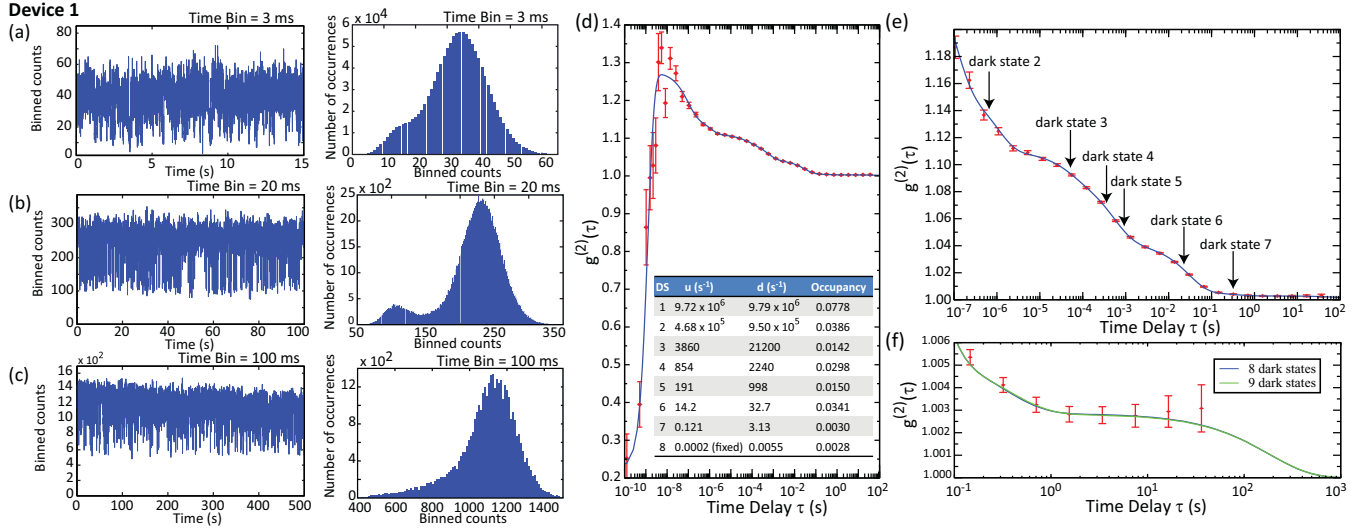


FIG. 2. (Color online) Device 1 data. Time-trace (left) and histogram data (right) for (a) 3 ms, (b) 20 ms, and (c) 100 ms time bins. (d)  $g^{(2)}(\tau)$ ; red points: experimental data; blue solid line: nonlinear least-squares fit to the  $N$  dark state model in Fig. 1(b), with  $N = 8$ . Inset table: fit values for excitation ( $u$ ) and decay ( $d$ ) rates and occupancy of each dark state (DS). (e) Same as (d), but zoomed in to the region between  $\tau = 100$  ns and  $\tau = 100$  s. Times  $\tau_i = 1/(u_i + d_i)$  are used as labels for the dark states, approximately indicating the locations of maximal slope in a plot of  $g^{(2)}(\tau)$  vs  $\log(\tau)$ . (f) Comparison of model for  $N = 8$  and  $N = 9$ , in the region between  $\tau = 10$  ms and  $\tau = 1000$  s. Within the region for which experimental data is available, no significant difference is seen for  $N > 8$ . The estimated QD radiative efficiency is 78%.

to hundreds of milliseconds. One physical picture qualitatively consistent with this observation would be that blinking is caused by the tunneling of carriers between the QD and several adjacent traps of varying separation from the QD. For example, Sercel and colleagues have considered electron relaxation from a QD through a deep level trap [33,34], and calculated that tunneling rates can vary by several orders of magnitude over a few tens of nanometers of QD-trap separation (see Supplemental Material for a plot of these tunneling rates). Such deep level traps may arise during the QD growth process itself [33,35,36] and may physically correspond to impurities, such as vacancies, antisites, and interstitials, produced during growth and postgrowth fabrication processes. We point out that a rapid thermal annealing step was used to blueshift the QD emission in our wafers [21,37], prior to device fabrication.

The estimated total dark state occupancy is 21.6%, so the radiative transition is still dominantly preferred over excitation into the dark states, with a radiative quantum yield of 78.4%. Finally, we note that the rates  $u_i$  and  $d_i$  for populating/depopping dark state  $i$  can at least be qualitatively linked to the location of prominent features in the  $g^{(2)}(\tau)$  data. For example, in a system consisting of a single dark state that is populated and depopulated at rates  $u_1$  and  $d_1$ , the slope of  $g^{(2)}(\tau)$  plotted vs  $\log(\tau)$  is maximal at  $\tau = 1/(u_1 + d_1)$  [18]. In a system comprised of multiple dark states, if excitation and decay rates are sufficiently different, the values  $\tau_i = 1/(u_i + d_i)$  still approximately point to slope maxima. Figure 2(e) identifies these points, which qualitatively match the experimentally observed maximum slope points. Quantitative details are given in [21].

Repeating this analysis for device 2 yields the results in Fig. 3. Here, neither time-trace nor histogram data show clear evidence of blinking. In contrast,  $g^{(2)}(\tau)$  in Fig. 3(c)

again provides evidence of bunching at the 10 ns time scale, followed by a series of shoulders, before reaching a value of unity. The data is fit to a rate equation model with five

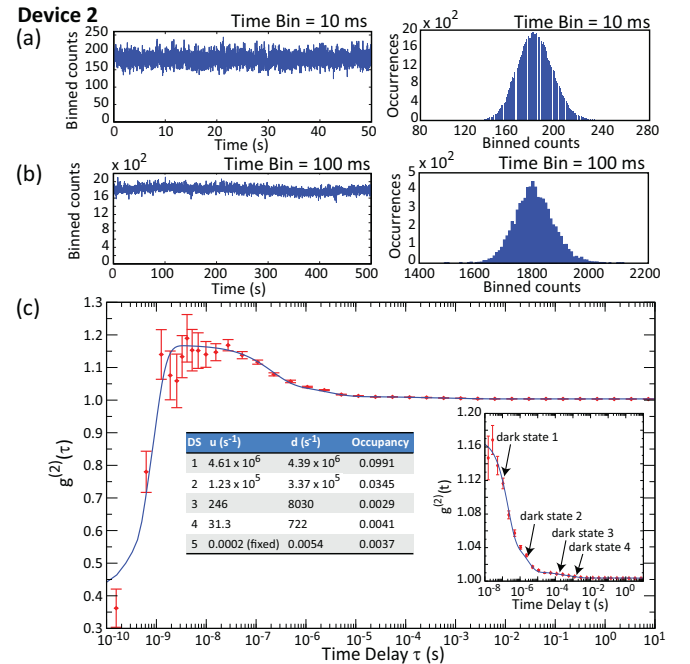


FIG. 3. (Color online) Device 2 data. Time-trace (left) and histogram data (right) for (a) 10 ms and (b) 100 ms time bins. (c)  $g^{(2)}(\tau)$ ; red points: experimental data; blue solid line: nonlinear least-squares fit to the model with  $N = 5$ . Inset table: fit values for excitation ( $u$ ) and decay ( $d$ ) rates, and occupancy of each dark state (DS). Inset graph: data over  $\tau = [10$  ns, 10 s]. Points  $\tau_i = 1/(u_i + d_i)$  are indicated for each dark state. The estimated QD radiative efficiency is 86%.

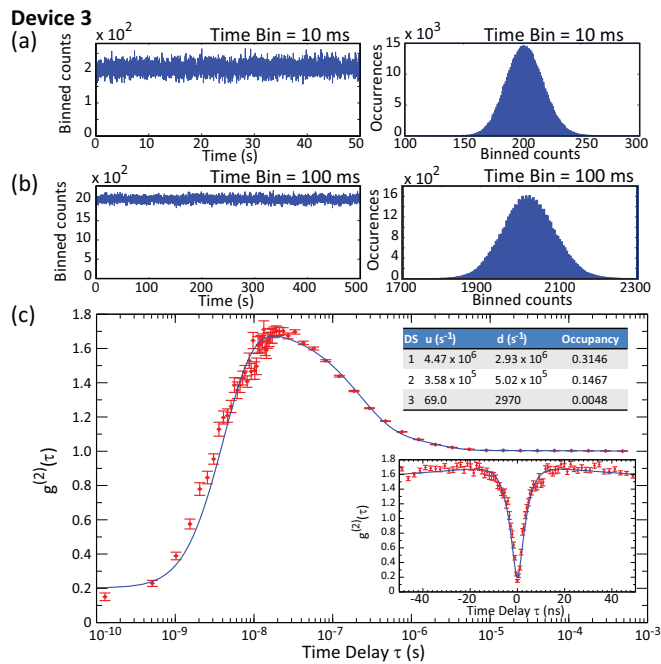


FIG. 4. (Color online) Device 3 data. Time-trace (left) and histogram data (right) for (a) 10 ms and (b) 100 ms time bins. (c)  $g^{(2)}(\tau)$ ; red points: experimental data; blue solid line: nonlinear least-squares fit to the model with  $N = 3$ . Inset table: fit values for excitation ( $u$ ) and decay ( $d$ ) rates and occupancy of each dark state (DS). Inset plot: data with linear time scale showing the antibunching dip at  $\tau = 0$ ; the pronounced photon bunching away from zero delay is not evident on this scale. The estimated QD radiative efficiency is 53%.

dark states, and again shows close correspondence [inset to Fig. 3(c)]. Contrasting with device 1, blinking at longer times (e.g.,  $> 10 \mu s$ ) is significantly less pronounced, and the estimated total dark state occupancy is 14.4%.

Finally, we present data from device 3 in Fig. 4. Similar to device 2, the time trace and histogram data show little evidence of blinking. The  $g^{(2)}(\tau)$  data does reveal significant blinking over submicrosecond time scales, but at longer times blinking is minimal and the system can be well fit to a model with  $N = 3$  (with final state occupancy  $< 0.5\%$ ). Interestingly, the total dark state occupancy is 46.7%, significantly greater than observed in either device 1 or 2. Thus, despite qualitative similarity with the time trace and histogram data of device 2, the dynamics of the QD are in fact qualitatively different, as revealed by the photon correlation measurements. This qualitative difference is perhaps unsurprising given its entirely

different device history (different wafer growth; no rapid thermal annealing [21]). Also, as the pronounced bunching persists out to microsecond time scales, an accurate estimate of  $g^{(2)}(0)$ , needed for assessing the purity of the single-photon source, requires acquisition and analysis of data out to many orders of magnitude longer times than the characteristic time scale of the antibunching dip.

Correlation functions can reveal the kinetics of the blinking signal over a large time range; however, only in a time-averaged sense [18]. Information about instantaneous intensity fluctuations, such as probability distributions for bright and dark intervals, can be obtained from photon-counting histograms, as commonly done in the blinking literature [8,18,23]. Applied to epitaxially grown QDs, this type of analysis has revealed exponential blinking time distributions [12–14], suggesting modification of the QD fluorescence by one or a few neighboring centers, as discussed (nanocrystal QDs have in contrast been shown to display power-law distributions [23]). We have applied this technique to the QD in device 1. Although our measured data does not strictly follow the stringent criteria suggested in [23] for reliable parameter extraction, we see strong indications of exponential probability distributions [21].

In summary, photon correlation measurements taken over 11 orders of magnitude in time are used to study blinking in epitaxially grown, self-assembled InAs QDs housed in photonic nanocavities. The measurements are fitted to a rate equation model consisting of a radiative transition coupled to a number of dark states. The model reproduces the observed behavior, allowing us to quantify the multiple blinking time scales present and estimate the QD radiative efficiency, which ranges between 53% and 85%. We anticipate that this approach will be valuable in studying the behavior of InAs QDs in proximity ( $< 100$  nm) to etched surfaces and/or metals in nanophotonic/nanoplasmonic geometries. Indeed, the blinking observed here may stem from traps produced in the fabrication of the nanostructures used to enhance QD emission collection. Measuring photon correlations across this broad range of time scales both before and after nanofabrication may help elucidate the origin of blinking in these systems.

C.S.H. acknowledges the CNST Visiting Fellow program and support from the Office of Naval Research through the Naval Research Laboratory's Basic Research Program. M.D. and S.A. acknowledge support under the Cooperative Research Agreement between the University of Maryland and NIST-CNST, Award No. 70NANB10H193.

[1] *Single Quantum Dots*, edited by P. Michler (Springer Verlag, Berlin, 2003).  
 [2] J. L. O'Brien, A. Furusawa, and J. Vučković, *Nat. Photonics* **3**, 687 (2009).  
 [3] P. A. Dalgarno, J. M. Smith, J. McFarlane, B. D. Gerardot, K. Karrai, A. Badolato, P. M. Petroff, and R. J. Warburton, *Phys. Rev. B* **77**, 245311 (2008).  
 [4] J.-M. Gérard and B. Gayral, *J. Lightwave Tech.* **17**, 2089 (1999).

[5] W. L. Barnes, G. Björk, J. M. Gérard, P. Jonsson, J. A. E. Wasey, P. T. Worthing, and V. Zwiller, *Eur. Phys. J. D* **18**, 197 (2002).  
 [6] M. Nirmal, B. O. Dabbousi, M. G. Bawendi, J. J. Macklin, J. K. Trautman, T. D. Harris, and L. E. Brus, *Nature (London)* **383**, 802 (1996).  
 [7] M. Kuno, D. P. Fromm, H. F. Hamann, A. Gallagher, and D. J. Nesbitt, *J. Chem. Phys.* **112**, 3117 (2000).

- [8] F. D. Stefani, J. P. Hoogenboom, and E. Barkai, *Phys. Today* **62**(2), 34 (2009).
- [9] P. Frantsuzov, M. Kuno, B. Janko, and R. A. Marcus, *Nat. Phys.* **4**, 519 (2008).
- [10] B. Lounis and M. Orrit, *Rep. Prog. Phys.* **68**, 1129 (2005).
- [11] *Single Semiconductor Quantum Dots*, edited by P. Michler (Springer-Verlag, Berlin, 2009).
- [12] X. Y. Wang, W. Q. Ma, J. Y. Zhang, G. J. Salamo, M. Xiao, and C. K. Shih, *Nano Lett.* **5**, 1873 (2005).
- [13] M.-E. Pistol, P. Castrillo, D. Hessman, J. A. Prieto, and L. Samuelson, *Phys. Rev. B* **59**, 10725 (1999).
- [14] M. Sugisaki, H.-W. Ren, K. Nishi, and Y. Masumoto, *Phys. Rev. Lett.* **86**, 4883 (2001).
- [15] C. Santori, D. Fattal, J. Vuckovic, G. S. Solomon, E. Waks, and Y. Yamamoto, *Phys. Rev. B* **69**, 205324 (2004).
- [16] M. Davanço, M. T. Rakher, D. Schuh, A. Badolato, and K. Srinivasan, *Appl. Phys. Lett.* **99**, 041102 (2011).
- [17] S. Ates, L. Sapienza, M. Davanço, A. Badolato, and K. Srinivasan, *IEEE J. Sel. Top. Quantum Electron.* **18**, 1711 (2012).
- [18] M. Lippitz, F. Kulzer, and M. Orrit, *Chem. Phys. Chem.* **6**, 770 (2005).
- [19] C. F. Wang, A. Badolato, I. Wilson-Rae, P. M. Petroff, E. Hu, J. Urayama, and A. Imamoglu, *Appl. Phys. Lett.* **85**, 3423 (2004).
- [20] S. Ates, I. Agha, A. Gulinatti, I. Rech, A. Badolato, and K. Srinivasan, *Sci. Rep.* **3**, 1397 (2013).
- [21] See Supplemental Material at <http://link.aps.org/supplemental/10.1103/PhysRevB.89.161303> for details regarding the device fabrication, fluorescence spectra, calculation of  $g^{(2)}(\tau)$  from the measured time tagged data, the rate equation model used to fit the experimental  $g^{(2)}(\tau)$  data, labeling of the dark states, and on/off time distribution data.
- [22] R. Verberk and M. Orrit, *J. Chem. Phys.* **119**, 2214 (2003).
- [23] C. H. Crouch, O. Sauter, X. Wu, R. Purcell, C. Querner, M. Drndic, and M. Pelton, *Nano Lett.* **10**, 1692 (2010).
- [24] T. A. Laurence, S. Fore, and T. Huser, *Opt. Lett.* **31**, 829 (2006).
- [25] A. Zumbusch, L. Fleury, R. Brown, J. Bernard, and M. Orrit, *Phys. Rev. Lett.* **70**, 3584 (1993).
- [26] L. Fleury, A. Zumbusch, M. Orrit, R. Brown, and J. Bernard, *J. Lumin.* **56**, 15 (1993).
- [27] A. Berthelot, I. Favero, G. Cassabois, C. Voisin, C. Delalande, P. Roussignol, R. Ferreira, and J. M. Gérard, *Nat. Phys.* **2**, 759 (2006).
- [28] M. Abbarchi, T. Kuroda, T. Mano, M. Gurioli, and K. Sakoda, *Phys. Rev. B* **86**, 115330 (2012).
- [29] A. N. Vamivakas, Y. Zhao, S. Fält, A. Badolato, J. M. Taylor, and M. Atatüre, *Phys. Rev. Lett.* **107**, 166802 (2011).
- [30] J. Houel, A. V. Kuhlmann, L. Greuter, F. Xue, M. Poggio, B. D. Gerardot, P. A. Dalgarno, A. Badolato, P. M. Petroff, A. Ludwig, D. Reuter, A. D. Wieck, and R. J. Warburton, *Phys. Rev. Lett.* **108**, 107401 (2012).
- [31] P. Spinicelli, S. Buil, X. Quélin, B. Mahler, B. Dubertret, and J.-P. Hermier, *Phys. Rev. Lett.* **102**, 136801 (2009).
- [32] T. Volz, A. Reinhard, M. Winger, A. Badolato, K. J. Hennessy, E. L. Hu, and A. Imamoglu, *Nat. Photonics* **6**, 607 (2012).
- [33] P. C. Sercel, *Phys. Rev. B* **51**, 14532 (1995).
- [34] D. F. Schroeter, D. J. Griffiths, and P. C. Sercel, *Phys. Rev. B* **54**, 1486 (1996).
- [35] S. W. Lin, C. Balocco, M. Missous, A. R. Peaker, and A. M. Song, *Phys. Rev. B* **72**, 165302 (2005).
- [36] T. Asano, Z. Fang, and A. Madhukar, *J. Appl. Phys.* **107**, 073111 (2010).
- [37] S. W. Lin, A. M. Song, N. Rigopolis, B. Hamilton, A. R. Peaker, and M. Missous, *J. Appl. Phys.* **100**, 043703 (2006).